11. AIR ION MEASUREMENTS AS A SOURCE OF INFORMATION ABOUT ATMOSPHERIC AEROSOLS

11.1. Introduction

The intermediate and large air ions represent charged aerosol particles in a diameter range approximately from 2 to 80 nm. Since the mobility and diameter of the particles are well correlated to each other, the mobility spectra contain essential information about aerosol particles, and the interpretation of the mobility spectra in terms of particle sizes could contribute to other fields of atmospheric science. *Junge* [1955] especially emphasized the significance of this approach for the nanometer size range, developed the corresponding theory, and performed a conversion of a few ion spectra to particle distributions. Unfortunately, the applied theoretical model of the attachment of small ions to aerosol particles was very rough for the nanometer size range. Several researchers have attempted to advance in this direction later (e.g. *Misaki* [1964], *Misaki et al*. [1972], *Dhanorkar and Kamra* [1993a], *Hõrrak et al.* [1996]). The procedure of transformation is similar to the procedure of data inversion in electric aerosol spectrometers, when the bipolar charging is used [*Liu and Pui*, 1975; *Hoppel*, 1978]. The specificity of atmospheric electric data is that the process of particle charging is not controlled; the controlling is a rule in aerosol spectrometers.

The procedures of conversion between mobility distribution and size distribution are based on two physical models: (1) the correlation between the mobility and size of a particle; (2) the charge distribution of particles. As to the first model, the state of affairs may be assessed as satisfactory: the Stokes-Cunningham-Millikan equation is sufficiently accurate above a particle diameter of 3 nm, and an improved procedure [*Tammet*, 1995] is available for smaller particles. The second model is much more problematic. The charge distribution of aerosol particles in a bipolar ion environment has been studied by many researchers (e.g. *Fuchs* [1947, 1963]; *Bricard* [1962]; *Hoppel and Frick* [1986, 1990]; *Reischl et al.* [1996]). However, the charge distribution on atmospheric aerosol particles is still unknown to a certain extent. The comparison of air ion mobility and aerosol particle size spectra in real atmosphere could fill this gap. This provides also information for assessing the rate of aerosol particle transformation during the evolution processes, when the charge distribution could be out of steady state, e.g., in the case of the nucleation bursts of nanometer particles [*Weber et al*., 1997, *Mäkelä et al*., 1997]. This also may give useful information about the generation mechanism (homogeneous nucleation or ion–induced nucleation) of newly arisen particles in the atmosphere. Experiments of this kind have been carried out in laboratory air (see references in paper *Kim et al*., 1997; 1998), but never in real atmosphere.

The procedures of conversion between mobility distribution and size distribution in atmospheric conditions have insufficient experimental proof. A complex test of two different conversion procedures, using simultaneous side-by-side atmospheric electric and aerosol measurements [*Hõrrak et al*., 1998a; 1988c], and the assessment of atmospheric electric measurements as a source of information about atmospheric aerosols is given in this section.

11.2. Measurements

The comparison measurements were carried out at Tahkuse Observatory from April 14 to May 16, 1994. The air ion spectrometer (AIS) covered the range of large and intermediate ions (mobility 0.00041–0.293 $cm^2V^{-1}s^{-1}$) that was roughly logarithmically divided into 9 fractions for each polarity (see Table 21). The corresponding size range of single-charged particle diameters is from 2.1 to 79 nm. Particles were measured as naturally charged in the bipolar atmospheric air. The concentration and mobility distribution of small ions (mobility 0.5–3.14 $cm^2V^{-1}s^{-1}$) of each polarity was simultaneously measured and recorded.

The Electric Aerosol Spectrometer (EAS) measured the distribution of particle concentrations in the diameter range of 0.01–10 μm. The spectrum was logarithmically distributed into 12 fractions (8 fractions are presented in Table 22). The data inversion algorithm in EAS, based on unipolar particle charging and mobility classification, is improved by experimental calibration by means of standard aerosols. Therefore, the EAS measurements are independent of atmospheric-electric air ion measurements, and the instrument can conventionally be considered as a directly calibrated instrument for the measurement of particle size spectra.

Both instruments were operated side by side during the test period with short interruptions for technical servicing. The air was sucked into the instrumentation through a wide metal channel and the samples into the AIS and into the EAS were taken at the same place at a height of about 5 m from the ground.

The measurement period was variable, with rather high concentrations of particles in the accumulation fraction (100–560 nm) in April, and low concentrations in May. Particularly in May, several aerosol episodes were observed with the bursts of ultrafine particles (10–18 nm) typically in the afternoons of fine weather (Figure 48). Simultaneously with the bursts of ultrafine particles depicted in Figure 48, the bursts of intermediate ions (mobility 0.034–0.5 $cm^2V^{-1}s^{-1}$; diameter 1.6–7.4 nm) were also observed. Unfortunately, this size range was left out of the scope of the EAS at that time.

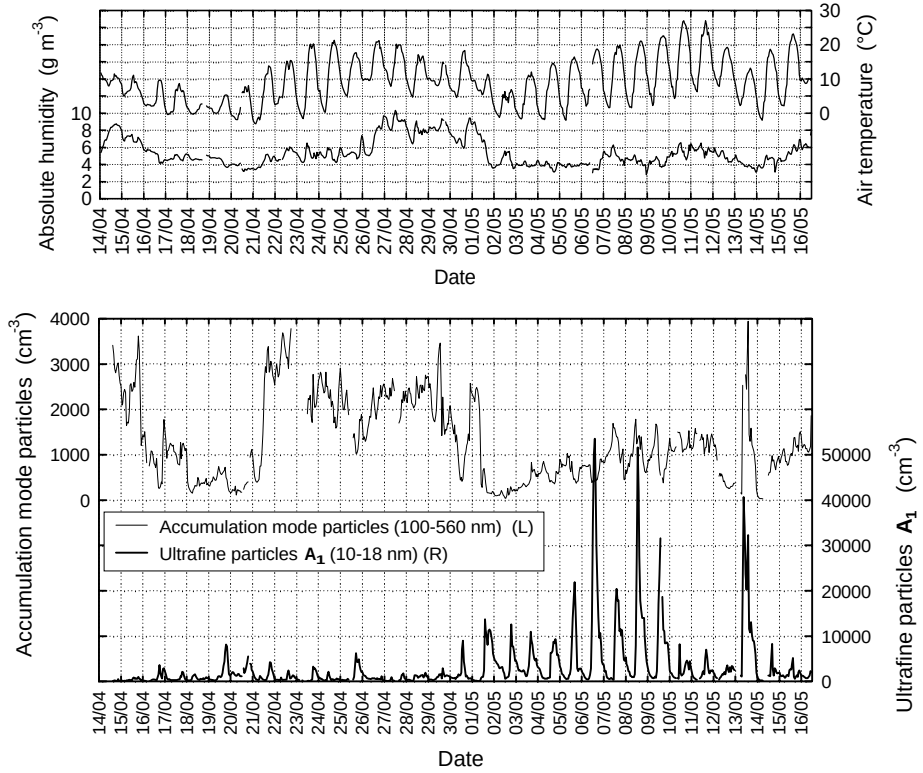

Figure 48. Time variation in the concentration of accumulation mode (100–560 nm) and ultrafine particles A_1 (10–18 nm), air temperature and absolute humidity.

According to aerosol situations, the monthly test period was divided into two subperiods called by convention the April period (April 14 – April 29) and the May period (April 30 – May 16). The two subperiods were discriminated by the beginning of the rapid increase in the formation of nanometer and ultrafine particles in atmospheric air on April 30. The intensive generation of particles followed the invasion of cool and clean Arctic high pressure air masses on May 1, when the particle concentration in the accumulation size range (100–560 nm) dropped from about 2400 cm^{-3} to 100 cm^{-3} (see Figure 48). The high pressure weather conditions prevailed almost all the time, the air pressure was below 1005 mb only on four days during the monthly period. The average air temperatures of two subperiods were 8ºC in April and 11ºC in May.

Table 21. Average mobility distributions of aerosol ion charge concentration measured using the air ion spectrometer. The corresponding diameter range of single-charged particles is shown in the second column.

Mobility	Diameter	Concentration of elementary charges (cm^{-3})			
Range	range	April		May	
($cm^2 V^{-1} s^{-1}$)	(nm)	+ ions	– ions	+ ions	– ions
0.150–0.293	2.1–3.2	5.3	5.6	11.7	12.8
0.074–0.150	3.2–4.8	8.8	8.7	22.4	22.4
0.034–0.074	4.8–7.4	19.2	19.5	53.0	52.2
0.016–0.034	7.4–11	35.4	33.0	99.7	94.0
0.0091–0.0205	9.7–15	86	86	236	234
0.0042–0.0091	15–22	138	143	320	325
0.00192–0.00420	22–34	244	247	450	456
0.00087–0.00192	34–50	468	457	664	658
0.00041–0.00087	50–79	671	677	683	684

The AIS was operated in a routine mode; the hourly average fraction concentrations were recorded. The average particle number size spectrum over an approximately nine-minute collection time was measured and recorded by the EAS every ten minutes. 331 hours in April and 329 hours in May, when both instruments were running in the standard regime and providing technically correct results, were considered when calculating averages. The average characteristics of small air ions for the two subperiods are shown in Table 23, and the average mobility and size distributions used in the following analysis are presented correspondingly in Tables 21 and 22.

Table 22. Average size distributions of aerosol particles measured by means of EAS.

Diameter range (nm)	Particle number concentration (cm^{-3})	
	April	May
10–18	1060	4918
18–32	1693	4542
32–56	2625	3962
56–100	2370	2063
100–178	1269	713
178–316	426	170
316–562	76	26
562–1000	8	6

Table 23. Average concentration (cm^{-3}) and mean mobility ($cm^2V^{-1}s^{-1}$) of positive and negative small air ions.

Quantity	Average values	
	April	May
Concentration (+)	229	309
Concentration (–)	190	272
Mean mobility (+)	1.38	1.27
Mean mobility (–)	1.55	1.43

11.3. Preliminary data analysis

The correlation and regression analyses were used to find the relationship between aerosol particles and air ions. In general, the hourly average concentrations of the air ion mobility fractions correlated very well with the corresponding aerosol particle size fractions (Table 24). There was almost no difference between negative and positive ions in the correlation with the aerosols. The concentrations of positive and negative air ion fractions were closely correlated; the correlation coefficients were 95.5–99.4%.

Table 24. Correlation coefficients (%) between aerosol and air ion mobility fractions. The equivalent diameter ranges of air ion mobility assume single-charged particles.

Air ions		Aerosol particle diameter range (nm)			
Mobility range ($cm^2 V^{-1} s^{-1}$)	Equivalent diameter (nm)	$\mathbf{A_1}$ 10–18	$\mathbf{A_2}$ 18–32	$\mathbf{A_3}$ 32–56	$\mathbf{A_4}$ 56–100
0.0091–0.0205	$\mathbf{J_1}$: 9.7–15	97	80	37	-8
0.0042–0.0091	$\mathbf{J_2}$: 15–22	96	91	52	1
0.00192–0.00420	$\mathbf{J_3}$: 22–34	80	98	77	21
0.00087–0.00192	$\mathbf{J_4}$: 34–52	37	75	96	56
0.00041–0.00087	$\mathbf{J_5}$: 52–79	-3	21	71	91

As the fraction boundaries of the EAS and the AIS do not coincide, we calculated the ion fraction concentrations ($\mathbf{I_i}$) for the mobility fractions coinciding with the size fractions of the EAS ($\mathbf{A_i}$), using the piece-wise linear approximation model of the ion mobility distribution density function. As an exception, the upper boundary of the largest fraction of aerosol particles $\mathbf{A_4}$ was reduced to 79 nm (Table 25). Despite the high correlation between the fraction concentrations, the ratios of $\mathbf{I_i}/\mathbf{A_i}$ commonly varied in the ranges of 5–15%, 10–20%, 15–30%, 17–35% for the aerosol fractions from $\mathbf{A_1}$ to $\mathbf{A_4}$, respectively. At the lowest concentrations of the fractions $\mathbf{A_1}$ and $\mathbf{A_2}$, a deviation from the above ranges to somewhat higher values was observed. The ratios of $\mathbf{I_i}/\mathbf{A_i}$ were found to be dependent on the aerosol particle concentration: the lower values corresponded to a higher concentration of aerosol particles.

If the mobility and size fractions are related by one-to-one, then the ratio of the fraction concentrations $\mathbf{I_i}/\mathbf{A_i}$ gives the percentage of single-charged (positive or negative) particles, or the charging probability in the case of particles smaller than 50 nm; then percent of multiply charged particles is below 1%. The scatterplot between these two correlated variables can be fitted with a line of the linear regression function, the intercept of which should be zero, and the slope gives the mean charging probability for the fraction.

The results of the regression analysis commonly showed a linear correlation between the coinciding fractions of air ions and aerosol particles, but with a non-zero intercept (Figure 49). The step at the zero value of the fraction concentration (intercept) could be interpreted as an uncertainty due to the calibration of spectrometers, the procedure of converting the fractions into coinciding fractions, and also due to the effect of multiple charges on aerosol particles.

In the case of the first three fractions of aerosol particles ($\mathbf{A_1}$, $\mathbf{A_2}$ and $\mathbf{A_3}$) the non-zero intercept can be ignored (taking into account the entire range of variation), and the slope of regression function can be considered as the average charging probability of the fraction. These results presented in Table 25 are generally in accordance with the steady state bipolar charging probabilities [*Hoppel et al.*, 1986; *Tammet*, 1991, *Reischl et al.*, 1996]. Consequently, the charging of these particles, concerning the hourly averaged data, displayed a nearly steady state character even in the case of the bursts. Some depletion of the charged fraction of $\mathbf{A_1}$ at high concentrations (see Figure 49) could indicate the aerosol evolution process, when the charge distribution differed from the steady state distribution because of the fast generation of particles. In such cases the increment of concentration was more than about 10000 cm^{-3} per hour. No systematic depletion of the charged fraction was recorded in the case of fractions $\mathbf{A_2}$ and $\mathbf{A_3}$. These fractions are considered to be in a quasi-steady state of charging with cluster ions in the rural environment, far away from big anthropogenic sources of pollution. The time variation in the concentration of air ion fraction $\mathbf{I_4}$ followed that of ultrafine particles $\mathbf{A_4}$, in general. The effect of multiple charges, which is assumed to be significant in the case of large particles (>50 nm), did not disturb the general variation. About 5% of aerosol particles of the size of 100 nm have double charges [*Hoppel et al*., 1986]. The particles with double or multiple charges may affect the ion mobility fraction $\mathbf{I_4}$.

Our recent study [*Tamm et al*., 2001] showed the linear correlation between the concentrations of air ions and aerosol particles down to the smallest fraction of 3.2–5.6 nm measured by the new version of EAS. Preliminary estimates of the charging probabilities of the aerosol particles with diameters below 10 nm are higher than in the stationary case.

Table 25. Correlation coefficients between the concentrations of air ions and aerosol particles in coinciding fractions, the slopes of regression functions between fractions, and the steady state charging probability of a single charge on the particle for the geometric mean diameters of the fractions.

Diameter range (nm)	Mobility range ($cm^2V^{-1}s^{-1}$)	Correlation between fractions $\mathbf{I_i}$ and $\mathbf{A_i}$, (%)	Slope of regression line	Charging probability
$\mathbf{A_1}$: 10–18	$\mathbf{I_1}$: 0.00638–0.0188	98	0.066	0.074
$\mathbf{A_2}$: 18–32	$\mathbf{I_2}$: 0.00216–0.00638	97	0.10	0.13
$\mathbf{A_3}$: 32–56	$\mathbf{I_3}$: 0.00074–0.00216	96	0.19	0.19
$\mathbf{A_4}$: 56–79	$\mathbf{I_4}$: 0.00041–0.00074	93	0.31	0.23

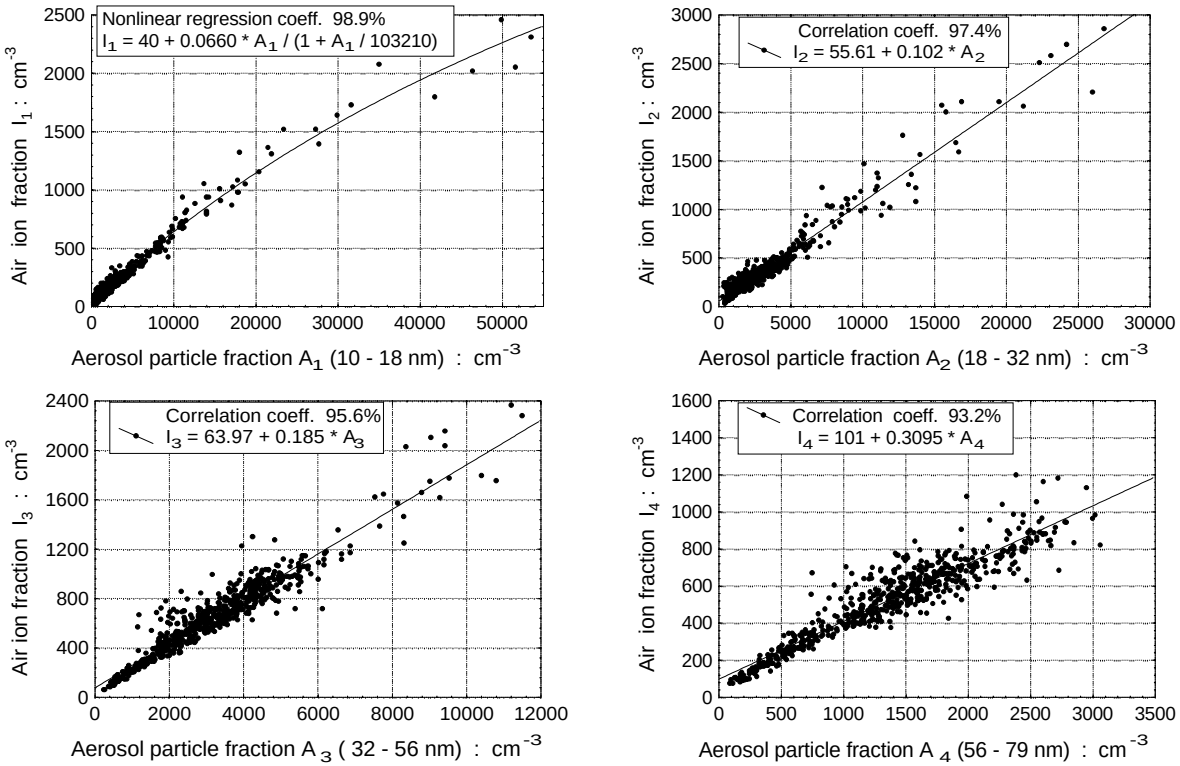

Figure 49. Scatterplots of the aerosol particle concentration A_1 (10–18 nm) versus charged fraction concentration I_1 (air ions with mobilities of 0.00638–0.0188 $cm^2V^{-1}s^{-1}$), A_2 (18–32 nm) versus I_2 (0.00216–0.00638 $cm^2V^{-1}s^{-1}$), A_3 (32–56 nm) versus I_3 (0.000741–0.00216 $cm^2V^{-1}s^{-1}$), and A_4 (56–78 nm) versus I_4 (0.000405–0.000741 $cm^2V^{-1}s^{-1}$).

11.4. Transformation of the spectra

The mobility spectrum of large air ion space charge $\rho(Z) = \mathrm{d}\rho/\mathrm{d}Z$ and the size distribution of the particle number concentration $n(r) = \mathrm{d}n/\mathrm{d}r$ are related by the equation (e.g., *Salm*, 1988)

$$\rho(Z) = e\sum_{q=1}^{\infty} q\, n(r_{qZ})\, p_q(r_{qZ}) \left|\frac{\mathrm{d}\,r}{\mathrm{d}\,Z}\right|_{rqZ}, \qquad (8)$$

where q is the number of elementary charges, r_{qZ} is the radius of an aerosol particle that corresponds to the prearranged values of Z and q, $p_q(r_{qZ})$ is the probability of carrying q elementary charges, and $|\mathrm{d}r/\mathrm{d}Z|_{rqZ}$ is the Jacobian of the transformation of the differential distribution function of air ions from r-space to Z-space at a known radius r_{qZ}.

The probability of carrying q elementary charges $p_q(r)$ or the charge distribution of a particle is the most problematic quantity in the conversion of mobility spectra into size spectra of particles. The establishment of the probability is complicated even in controlled conditions. In real atmosphere, the negative and positive small ions arise in equal numbers, and the model of bipolar diffusion charging of aerosol particles may be acceptable. However, the concentration of aerosol particles exhibits considerable variations. Obviously, the assumption of steady state charging is sufficiently correct only for values averaged over periods that are many times longer than the characteristic evolution time (about one hour).

In the first approximation, we assume a steady state bipolar charging and consider a long period of two weeks for checking with measurements. First of all, the model for charge distribution is based on the expression for attachment coefficient of a small ion to an aerosol particle by *Fuchs* [1947]

$$\beta_q^{\circ}(r) = 4\pi r D x / [\exp(x) - 1]\,, \qquad (9)$$

where D is the diffusion coefficient, $x = qe^2/(4\pi r\varepsilon_o KT)$, ε_o is the electric constant, K is the Boltzmann constant, and T is the temperature. Eq. 9 is exact for particle radii above about 100 nm. For smaller particles, only sophisticated algorithms or numerical tables are available. Since extreme accuracy is not necessary in the present study, we used the algorithm by *Tammet* [1991] that approximates the tabulated results of *Hoppel and Frick* [1990]:

$$\beta_q(r) = (1 - 2\ /\ (2 + q(q-1) + r\ /\ 5\ \mathrm{nm}))\ \beta_q^{\circ}(r)\,. \qquad (10)$$

The algorithm was improved: the correction factor $(1 - 2\ /(2 + q(q-1) + r\ /5$ nm)) was replaced by the square root of the same factor that provides better agreement between the algorithm and recent experimental data [*Reischl et al.*, 1996]. The probability $p_q(r)$ for the steady state is calculated in the known way using the equation of balance for q-charged fractions of particles considering symmetrical bipolar charging [*Hoppel and Frick*, 1986; *Tammet*, 1991]. The function $Z(r)$ is calculated by means of the Stokes-Cunningham-Millikan equation [*Tammet*, 1995].

If the mobility spectrum is measured, the inverse problem has to be solved to find the size spectrum of aerosol particles $n(r)$. The infinite-dimensional Eq. 8 cannot be immediately solved. Thus, it should be replaced by a finite-dimensional equation in the stage of data processing. Two alternative techniques are considered. In the first occasion both the particle size spectrum and the air ion mobility spectrum are described by finite-dimensional fraction models and Eq. 8 is replaced by an algebraic equation (method developed by *Tammet* [1980, 1991, 1995])

$$c_i = \sum_{j=1}^{k} H_{ij} n_j \qquad (11)$$

where c_i denotes the number concentrations of elementary charges in air ion mobility fractions and n_j denotes the number concentrations of particles in aerosol size fractions. The elements of the transformation matrix H can be evaluated according to the equation

$$H_{ij} = \frac{1}{r_j^+ - r_j^-} \sum_{q=1}^{\infty} \int_{r_j^-}^{r_j^+} \begin{Bmatrix} \text{if } \ Z(q,r) \in \left(Z_i^- \ldots Z_i^+\right) \text{ then } \ q p_q(r) \\ \text{else} \qquad\qquad\qquad\quad 0 \end{Bmatrix} \mathrm{d}\,r\ , \qquad (12)$$

where r_j^-, r_j^+, Z_i^-, and Z_i^+ are lower and upper boundaries of the size and mobility fractions.

In the second occasion, the calculated aerosol particle size spectrum is represented by a simple parametric model. The KL-model [*Tammet*, 1988, 1992b] was chosen to fit the data:

$$\frac{\mathrm{d}\,n}{\mathrm{d}(\ln r)} = r\,n(r) = \frac{a}{\left(r/r_x\right)^K + \left(r_x/r\right)^L}\ . \qquad (13)$$

The size spectrum is described by the values of four parameters a, r_x, K, and L in the model: L is ascent of the left asymptote, K is descent of the right asymptote of the KL-distribution. The parameters a, r_x are the y-coordinate and x-coordinate of the intersection of asymptotes, respectively. If the aerosol size spectrum $n(r)$ in Eq. 8 is replaced by the expression of the KL-distribution, the equation will contain four unknown scalar quantities. The values of the parameters can be estimated according to the principle of least square fitting of the mobility spectra.

The aerosol particle size distributions measured by the EAS and calculated from intermediate and large air ion measurements according to the fraction model (Eq. 11) are presented in Figure 50. Size fractions for ion spectrometer were chosen so that their limits corresponded to the mobility limits of the single-charged air ion mobility fractions (fractions 1–8 in Table 21). The positive and negative polar conductivities of the air were nearly equal during both measuring periods. Thus, the values of the function $p_q(r)$ were calculated assuming the symmetrical charging and the average values of positive and negative large ion concentrations were used when solving Eq. 11. The values of the fraction concentration were converted to the values of the distribution function using interpolation between the fractions. The disagreement between the results obtained by directly calibrated (EAS) and indirect (ion spectrometer) method is not large and can be explained by uncertainties in the calibration of the instruments. The same conclusion was confirmed when comparing the data using the KL-model presentation of the particle size spectra.

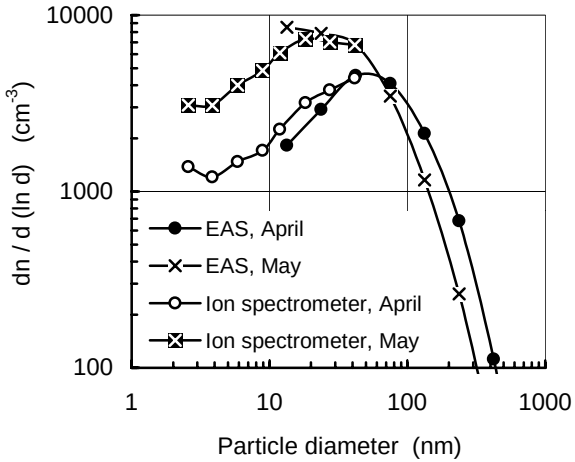

Figure 50. Size distribution of atmospheric aerosol at Tahkuse measured by means of EAS and calculated on the basis of Eqs. 11 and 12 according to intermediate and large air ion measurements.

The size distributions of aerosol particle measured by the EAS and calculated from large air ion measurements using the KL-model (Eq. 13) are presented in Figure 51. The estimated KL parameters have values respectively in April period: K = 2.71, L = 0.643, a = 8230 cm^{-3}, r_x = 42.2 nm and in May period: K = 2.65, L = 0.471, a = 11930 cm^{-3}, r_x = 30.5 nm. In this case the first air ion mobility fraction in Table 21 is not taken into account, since it deviates from the left asymptote determined by other fractions. Due to a low upper limit of the particle diameter (79 nm) for the air ion spectrometer the convergence of the determination of the value of parameter K is not satisfactory. In the present paper, the values of K have been corrected according to the spectra measured by the EAS. The KL-model is suitable for the approximation of smoothed size spectra of aerosol particles, when the fine structure of spectra is not essential, especially for number distribution in continental air [*Kikas et al.*, 1996].

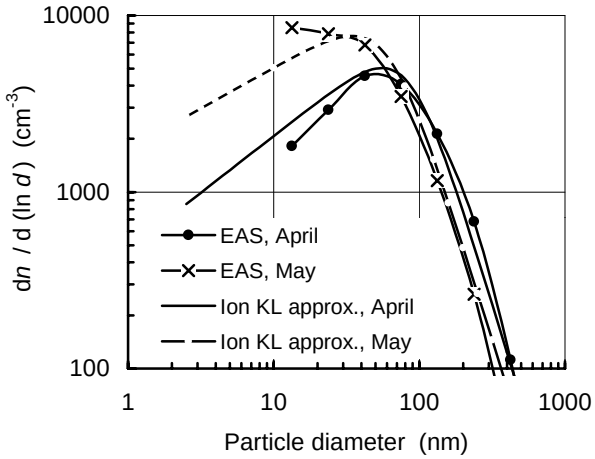

Figure 51. Size distribution of atmospheric aerosol at Tahkuse measured by means of EAS and calculated according to large air ion measurements using the KL-model.

A peculiarity of the results is that the data points situated at the left edge at 2.6 nm in Figure 50 are higher than expected according to the general regularities in the particle size spectra. We assume that the presented calculations are not correct in a particle diameter range below 3 nm due to the non-equilibrium charging of very small particles in the atmospheric air. The age of such particles is too short to reach the equilibrium that is expected in the used algorithm of the function $p_q(r)$. If the particle would be born in the neutral status, data points in the extreme left in Figure 50 should be lower than the extrapolated curve. The opposite position of these data points indicates that a number of nanometer particles probably are born in the charged status and the ion-induced nucleation should be considered as a mechanism of gas-to-particle conversion in atmospheric air. This is also in accordance with the results of our recent measurements of air ions and nanometer aerosol particles in the size range of 3.2–18 nm [*Tamm et al.*, 2001].